Photoproduction of the Very Strangest Baryons on the Proton target in CLAS12

A. Afanasev, W.J. Briscoe, H. Haberzettl, I.I. Strakovsky*, and R.L. Workman

The George Washington University, Washington, DC 20052, USA

M.J. Amaryan and G. Gavalian

Old Dominion University, Norfolk, Virginia 23529, USA

Ya.I. Azimov

Petersburg Nuclear Physics Institute, Gatchina, Russia 188300

M. Battaglieri and R. De Vita

INFN, Sezione di Genova, 16146 Genova, Italy

V.N. Baturin, V. Kubarovsky, E. Pasyuk*, S. Stepanyan, D.P. Weygand, and V. Ziegler*

Thomas Jefferson National Accelerator Facility, Newport News, VA 23606, USA

J. Bono and L. Guo*,**

Florida International University, Miami, FL 33199, USA

M. Dugger*

Arizona State University, Tempe, Arizona 85287-1504, USA

J. Goetz* and B.M.K. Nefkens

University of California at Los Angeles, Los Angeles, CA 90095, USA

D. Glazier and D.P. Watts*

Edinburgh University, Edinburgh EH9 3JZ, United Kingdom

D.G. Ireland and K. Livingston

University of Glasgow, Glasgow G12 8QQ, United Kingdom

F.J. Klein

Catholic University of America, Washington, DC 20064, USA

A. Kubarovsky

Rensselaer Polytechnic Institute, Troy, New York 12180-3590, USA

K. Nakayama

University of Georgia, Athens, GA 30602, USA

Yongseok Oh

Kyungpook National University, Daegu 702-701, Republic of Korea

J.W. Price

California State University, Dominguez Hills, Carson, CA 90747, USA

W. Roberts

Florida State University, Tallahassee, FL 32306, USA

C. Salgado

Norfolk State University, Norfolk, VA 23504, USA

V. Shklyar

Giessen University, D-35392 Giessen, Germany

(The Very Strange Collaboration)

** - Contact person, * - Spokesperson

(Dated: March 30, 2012)

Abstract

Almost half a century after the prediction and discovery of the Ω^- baryon, many properties of the $S = -2$ and -3 hyperon resonances remain unknown. In particular, recent theoretical predictions suggest there are many more Cascade states than have been seen. The CLAS detector, part of JLAB's 6 GeV program, has provided a unique lens into photo-production of the lowest mass Cascade states at threshold, however the energy and luminosity reached was not sufficient to study the heavier Ξ^*'s or the Ω^-. With the increased energy and better charged-kaon identification promised with CLAS12, we propose to study the production mechanisms of $S = -2, -3$ baryons with high precision and statistics in exclusive photo-nuclear reactions.

The production mechanism of these states is of particular interest: the change of strangeness number is large from the initial state to the final state baryon, there is no current precision measurement of the differential cross section for the Ω^- and there is no polarization measurement of the cascades in photoproduction. The spin-parity of the few relatively well-established cascade states, such as $\Xi(1690)$ and $\Xi(1820)$, may be confirmed via the double moments analysis technique using the combined decay angular distributions. The improved CLAS12 detector acceptance for the few-particle final states, which is necessary for the detection of these baryons, makes it possible to access their production mechanisms.

The proposed experiment would be run in parallel with the approved CLAS12 meson spectroscopy experiment using the forward tagger currently under construction. This experiment is expected to yield the statistics necessary to perform the cross section measurements for the Ω^- baryon. In addition, the proposed experiment is expected to yield high statistics for Cascade baryons, corresponding to the world's largest sample for the Ξ ground state in photoproduction and allowing the possibility of discoveries of new excited Ξ-states, and the determination of their quantum numbers.

I. INTRODUCTION

Historically, baryons with multiple strange quarks have played an important role in the development of the quark model and our understanding of the universe. The prediction and discovery of the Ω^- baryon certainly was one of the great triumph of the quark model. However, half a century later, there have been little new information about the Ω and Ξ baryons. In fact, only two Ω states and six Ξ states are considered to be well-established, with at least three stars ratings in the PDG [1]. This dismal state is largely due to the difficulty of producing these baryons which typically have very small cross sections, and the gradual decommissioning of existing kaon and hyperon beam facilities. However, due to the intrinsic $s\bar{s}$ content of the photon beam, it has become clear that photon beam facilities, such as CLAS (and CLAS12 and GlueX in the future), could also produce these $S = -2, -3$ baryons with sufficient statistics in order to discover new states, determine their quantum numbers, as well as providing information about their production mechanisms by performing measurements of differential cross sections as well as polarization observables.

It is important to note that what makes these baryons so difficult to produce is also probably the main reason that it is so interesting to understand their production mechanisms. In the case of Ω^-, in order to produce them in photoproduction in a proton target, it is necessary to produce three $s\bar{s}$ pairs from the vacuum. Such a large change of the baryon strangeness from the initial state ($S = 0$) to final state ($S = -3$) makes it particular interesting to study its production mechanism. Similarly, for the Ξ baryons in photoproduction ($\Delta S = -2$), it remains unclear whether they are produced through the decay of intermediate $S = -1$ hyperons.

Although both Ξ and Ω baryons are typically much more difficult to produce, they are, however, usually much narrower and could be easier to identify. For Ξ excited states, they are typically $5 - 10$ times at least narrower than their $S = 0, -1$ counterparts. As for Ω excited states, although much is unknown about them, it is natural to expect that they will exhibit similar feature to the Ξ sectors.

With the expected improved acceptance of CLAS12 for multiple-particle final states, and an order of magnitude higher luminisoty than CLAS, and several GeV higher beam energies, it is very possible that many aspects of the Ω and Ξ physics can be probed at CLAS12 using the quasi-real photon beams with the forward tagger. In addiction to the cross section

measurments for the ground state Ω^- and Ξ baryons, CLAS12 is expected to provide sufficient statistics to perform polarization measurement for the Ξ^- baryon, which is important to understand its production mechanism. Due to the large acceptance for multiple-particle final state reactions, it could also become feasible to determine or confirm the spin-parity of multiple excited cascades because the whole decay chain could be reconstructed. In addition, the experimental verification of the excited cascade decoupling from the $\Xi\pi$ channel could provide fresh information about why the cascade resonances are so narrow, and a series of measurements on the mass-splitting of Ξ^* could deepen our understanding of the u/d quark mass difference.

II. PHYSICS MOTIVATION

A. Search for the Ω-states in Photoproduction

A distinctive feature of the photoproduction of strangenest baryons (Ω) is the fact that it represents the largest strangeness transfer possible, ΔS = 3. In terms if Ω photoproduction, our first goals are two-folded:

- Cross section measurements for $\gamma p \to \Omega^- K^+ K^+ K^0$ which is still unknown,
- Study of a mechanism of the Ω^- photoproduction which should be quite specific, since it is the first baryon with constituents none of which could come from the target proton.

Of course, if the proposed experiment succeeds, it would be natural to search for other excited Ω states. In fact, only the $\Omega^-(2250)$ states is rated with at three stars in PDG, while both $\Omega(2380)^-$ and $\Omega(2470)^-$ both have not been firmly established (Table 1).

The main limiting factors in any Ω experiment of this kind are the photoproduction cross section (i.e., rates) and the background, neither of which are known.

Despite the fact that its prediction and eventual discovery was one of the brightest highlights in hadron physics, not much is known about Ω^- properties and mechanism of the Ω^- production. Here are some basic facts:

- In 1962, Gell-Mann and Neâeman predicted a new baryon, Ω^-, with S = -3, $J^P = 3/2^+$, and the mass about 1670 MeV [2].

State	PDG rating	Width (MeV)	J^P
Ω^-	****		$\frac{3}{2}^+$
$\Omega(2250)^-$	***	55 ± 18	$\frac{?}{?}^?$
$\Omega(2380)^-$	**	26 ± 23	$\frac{?}{?}^?$
$\Omega(2470)^-$	**	72 ± 33	$\frac{?}{?}^?$

TABLE I: Well Established Cascade Resoances [1].

- The $\Omega(1670)^-$ observation in 1964 at BNL triumphantly confirmed the hypothesis of $SU(3)_F$. The unambiguous discovery in both production and decay was reported in Ref. [3]. They scan > 100k buble chamber pictures with 5−10 K^- per picture and found a single and unique Ω^--event.

- The quantum numbers follow from the assignment of the particle to the baryon decuplet. Ref. [4] ruled out $J = 1/2$ and find consistency with $J = 3/2$. The spin of the Ω-hyperon has been recently determined (though with some assumptions) by the BaBar Collaboration at SLAC [5]. They found from decay angular distributions of $\Xi_C^0 \to \Omega^- K^+$ and $\Omega_C^0 \to \Omega^- K^+$ that $J = 3/2$; this depends on the spins of the Ξ_C^0 and Ω_C^0 being $J = 1/2$, their supposed values. The parity of the $\Omega(1670)^-$ stays totally unknown.

- Cross sections of $\Omega(1670)^-$ production have been measured using kaon beams. The ANL experiment measured the $K^- p \to \Omega^- X$ cross section at 6.5 GeV/c as $\sigma_t = 1.4 \pm 0.6\ \mu b$ [6]. The experiment SLAC-E-135 forward differential cross section for $K^- p \to \Omega^- X$ at 11 GeV/c [7]. Experiment SLAC-BC-073 sought Ω-photoproduction in the $\gamma p \to \Omega^- X$ reaction at 20 GeV, and provided only an upper limit of $\sigma_t < 17$ nb [8].

Although there have been no experimental data on the photoproduction of Ω^-, other than the upper limit set by the SLAC experiment [8], various theoretical models by Roberts, Afanasev, and Shklyar have provided predictions of cross sections of Ω^- photproduction, typicall around 0.3 nb. (These predictions will be discussed in detail in later sections.) Therefore, we believe CLAS12 has an historical and unique opportunity to produce long-waited new data on Ω-resonances.

B. Missing Cascade States

1. *The missing cascade states*

According to the constituent quark models, there should be a cascade state for each corresponding N^* and Δ^* resonances. In fact, Isgur and Capstick predicted a total of 44 cascade states below 2.5 GeV, using a relativistic quark model with chromodynamics [9]. Compared with these predictions, the state of experimental data of cascade states is dismal. Overall, only 6 cascade states in the PDG are listed with three or four stars [1], while only three of them have their quantum numbers J^P considered determined (Table 2). This is largely due to the difficulty to produce cascade resonances with two strange quarks, and gradual unavailability of kaon beam facilities.

State	PDG rating	Width (MeV)	J^P
$\Xi(1320)$	****		$\frac{1}{2}^+$
$\Xi(1530)$	****	9.5	$\frac{3}{2}^+$
$\Xi(1690)$	***	< 30	$\frac{1}{2}^-$?
$\Xi(1820)$	***	24	$\frac{3}{2}^-$
$\Xi(1950)$	***	60	?
$\Xi(2030)$	***	20	$\frac{5}{2}^?$

TABLE II: Well Established Cascade Resoances[1].

In the past two decades, there have been no new cascade states discovered. The only new information comes from the measurement of $\Xi^0(1690) \to \Xi^-\pi^+$ by the W89 Collaboration, while $\Xi(1690)$ has only been observed to decay largely to $\Lambda/\Sigma K^-$ [13]. This result had two implication to us. The first is that although the statistics of the $\Xi\pi$ events used in the analysis was very high, they suffer from high combinatoric background from the inclusive reaction of $\Sigma^-(C, Cu) \to \Xi^-\pi+$. This problem could be avoided at CLAS12, due to the fact that these states can be produced and observed via exclusive reactions such as $\gamma p \to K^+K^+K^-\Lambda$ or $\gamma p \to K^+K^+\pi^-\Xi^0$. The second implication is that CLAS12, as opposed to the earlier results, could also simultaneously measure the different decay modes of excited cascade resonances. It is generally believed that the excited cascade states are in general much narrower than its

N^* and Y^* counterparts, and this is potentially due to the decay of $\Xi^* \to \Xi\pi$ is suppressed. Therefore, the experimental verification of excited cascades decay decouple from $\Xi\pi$ can provide very useful information in terms of the properties of the cascade spectrum, and in particular their unusually narrow widths, and CLAS12 could be a perfect venue to measure the branching ratios of the existing cascade resonances, even if no new states are discovered.

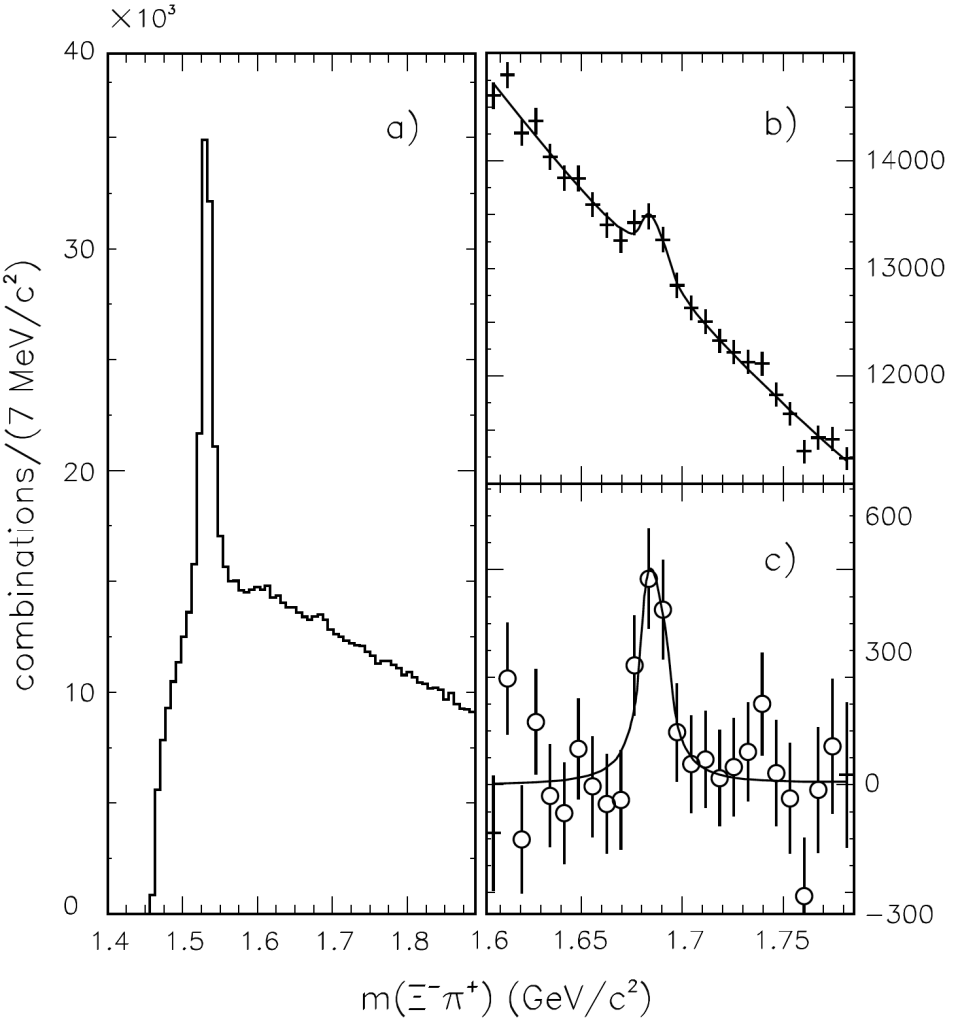

FIG. 1: Invariant mass distribution of the $\Xi^-\pi^+$ combinations in the reaction of $\Sigma^-(C, Cu) \to \Xi^-\pi+$ [13]. a)The $\Xi^0(1530)$ and $\Xi^0(1680)$ mass region; b) The $\Xi^0(1690)$ mass region only; c)the $\Xi^0(1690)$ mass region after background subtraction.

Although cascade cross section are typically one to two order of magnitude lower than hyperons, due to the necessity to produce another strange quark from the vacuum, the fact that the cascades are typically narrow makes it easier to identify the states if produced.

State	$BR(\rightarrow \Lambda\bar{K})$	$BR(\rightarrow \Sigma\bar{K})$	$BR(\rightarrow \Xi\pi)$
$\Xi(1530)$			100%
$\Xi(1690)$	seen	seen	seen
$\Xi(1820)$	large	small	small
$\Xi(1950)$	seen	seen?	seen
$\Xi(2030)$	20%	80%	small

TABLE III: Branching ratio of excited cascade resonances [1].

Furthermore, recent CLAS data have shown that the cascade resonances, such as $\Xi(1320)$ and $\Xi(1530)$, can be produced copiously with 1-2 GeV above threshold using a real photon beam at high luminosity. Although it must be noted that the comparison of cascade cross sections and those of hyperons are not necessarily fair and could be potentially misleading. Most hyperon cross sections exhibit dramatic decrease a few GeV away from threshold, while the cascade cross sections would not necessary have the same behavior, depending on the production mechanisms [10, 11]. The cross section of $\Xi^-(1320)$ in the exclusive reaction of $\gamma p \rightarrow K^+K^+\Xi^-(1320)$ increased from nb level around $E_\gamma = 3$ GeV to around 10 nb at 4 GeV [10]. Phenomenological models that hypothesize intermediate hyperons as the parent particle of Ξ, also do not predict the drop off of cross sections at higher energies [24]. Although recently published CLAS results consist of data using mostly photon energies below 4 GeV, a recent CLAS experiment (E05-017, also called $g12$ in this document [43]), have collected even higher statistic of cascade data, with beam energies up to 5.4 GeV, making it possible to study other excited cascade resonances. This CLAS experiment has an estimated luminosity of 28 pb^{-1} for $E_\gamma > 4.4$ GeV, using a 40 cm long hydrogen target.

Among the states listed in Table 3, there is recent evidence to suggest that $\Xi(1690)$ is a $J^P = \frac{1}{2}^-$ particle, from the decay $\Lambda_C^+ \rightarrow \Xi^-\pi^+K^+$ [12]. However, this result needed to make assumptions about the J^P of Λ_C^+ as well, making the independent measurement much desired. The $\Xi(1690)$ has mostly been seen in $Y\bar{K}$ decay, while the only notable sighting of $\Xi(1690) \rightarrow \Xi\pi$ with significant statistics was reported by [13]. This is a state that is of particular interest, as there already exist CLAS 6 GeV data with photon energies far enough from the threshold, making it possible to study $\Xi(1690)$ via both decay channels, and possibly determining their branching ratios, provide experimental verification of the $\Xi\pi$

suppression of Ξ^* decays. The proposed experiment at CLAS12 will greatly improve the statistics that is necessary for the J^P determination, which needs to reconstruct the whole decay chain.

As a sanity check, the reaction $\gamma p \to K^+K^+\pi^-(\Xi^0)$ has been analyzed recently using the g12 data set. The three charged particles in the final state are identified by CLAS, while the Ξ^0 is reconstructed using the missing mass technique. Although only 10% of the whole data set has been analyzed for this purpose, the quality of the data is very encouraging. The Ξ^0 signal is clearly visible above a constant background, mostly from events with pions misidentified as kaons. We expect to finalize various offline corrections, such as momentum corrections, beam energy corrections in the following semester, before we move on to analyze the whole data set. But it is clealy already the largest data set ever collected for cascade photoproduction. With at least two thousand $\Xi^0\pi$ events detected, equivalent to a factor of seven increase compared with previous results [10], a number of useful measurement previously unfeasible can now be performed.

First of all, we expect most of the $\Xi^0\pi$ events to be coming from the $\Xi^-(1530)$ decay. A possible background reaction is $\gamma p \to K^+K^{*0}\Xi^0$, although no known data is available. If out of the two thousand events, only 20% is from the decay of excited cascades, that it will still be significantly higher than any previous photoproduction data in this energy range. If these states are present in this data set, that it is highly likely that they can be identified due to the expected narrow widths. The differential cross section of $\Xi(1530)$ would certainly become feasible, which was not possible in the previous CLAS results due to much lower statistics at $E_\gamma > 4$ GeV. Such a study could provide important information about the production mechanisms of excited cascades, as opposed to ground states.

2. Mass splitting of Ξ doublets

Another unique feature of cascade physics is the possibility to perform the measurement of the mass splitting for multiple cascade doublets. In order to access the fundamental parameters of QCD such as quark masses, it is essential to perform the mass splitting of multiple baryon isospin multiplets. The average of the baryon ground state isospin multiplet ($N, \Sigma, \Delta, \Xi, \Sigma_c$, and Ξ_c) mass differences yields a value of $m_u - m_d = +2.8 \pm 0.3$ MeV/c^2 [45]. However, the Ξ ground state doublet mass splitting is the most intriguing one. The global

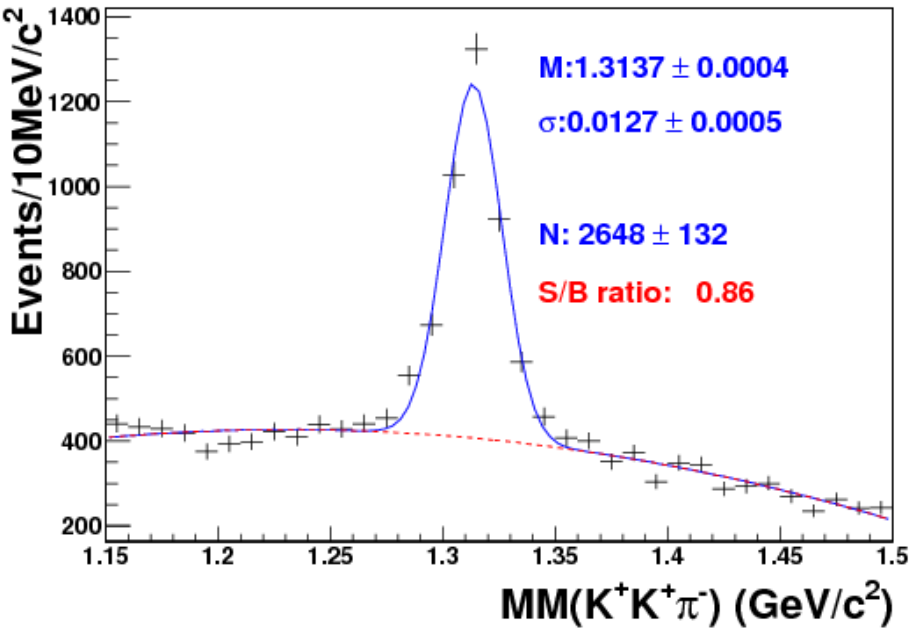

FIG. 2: The missing mass spectrum of the $K^+K^+\pi^-$ system off of a proton target, from the g12 experiment. The included photon energy range here is 3.3 GeV to 5.4 GeV [43]. Only 10% of the data have been analyzed and shown here. Various offline corrections, such as momentum corrections, beam energy corrections, have not been finalized for this experiment, and the parameters of the signal is expected to improve significantly.

average of the mass difference between the Ξ^0 and Ξ^- doublet is 6.48 ± 0.24 MeV/c^2 according to the PDG [1], significantly higher than that of the other baryon ground state multiplets. Recent QCD lattice calculation yield a result of 5.68 ± 0.24 MeV/c^2 [46], while a calculation based on radiative correction to the quark model gives a result of 6.10 MeV/c^2 [47]. Experimentally, however, it is important to point out that only one measurement of the Ξ^0 mass, by the NA48 Collaboration, has more than 50 events [48]. It seems plausible that this lone high statistics measurement of the Ξ^0 mass could be too low. In fact, recent CLAS measurement of the mass splitting of the ground state (Ξ^-, Ξ^0) doublet is 5.4 ± 1.8MeV/^{2} [10], which is lower than the global average. Nevertheless, the CLAS results did suffer from the lower statistics of the Ξ^0 events, and could not make a definite statement on the Ξ ground state doublet mass splitting.

CLAS12 would be well suited to perform multiple mass splitting measurements for a series of Ξ^* doublets, further enhancing our knowledge of the u, d quark mass difference.

This is largely due to the narrowness of the Ξ^* resonances, the improved acceptance and luminosity of CLAS12 than CLAS, and of course, the higher beam energy. These kind of multiple measurements of mass splitting of different baryon multiplets would not have been possible in other sectors such as N^* and Y^* resonances, due to their typical larger widths and the associated uncertainties.

C. Cascade Polarization

Hyperon polarization has generated much interest in the hadron physics community. Recently CLAS have produced several interesting results on the polarization of hyperons. In photoproduction data, Bardford et al. have shown that the Λ is 100% polarized with a circularly polarized photon beam [14] (Fig. 3, while the induced polarization of Λ in the reaction of $\gamma p \to K^+\Lambda$ is shown to change signs as a function of the K^+ center-of-mass angels [15] (Fig. 4). Similarly, due to the self-analyzing nature of the $\Xi(1320)$ weak decay, the polarization can be measured in various photo-nucleon reactions, with or without target/beam polarization. Such observables are important for the understanding of the production mechanism of cascade resonances in general. Furthermore, compared with the case of $\Lambda(uds)$, whose polarization is likely from the strange quark, with a small contribution from the (ud) diquark. the polarization mechanism of $\Xi((u/d)ss)$, however, might be totally different. The cascade polarization is more likely from the valence quark (u/d) instead of the (ss) diquark. If this is true, then the recoil polarization of Ξ should be negligible in photoproduction data without beam/target polarization, opposed to the sizable recoil polarization observed for Λ. It is also possible to use the polarization of the $\Xi(1320)$ in photoproduction on a polarizaed nucleon target to study the different contributions of valence quarks to the nucleon polarization, which would be complimentary to the results using electron scattering.

Because of parity conservation in the production of Ξ^- in the reaction of $\gamma p \to K^+K^+\Xi^-(1320)$, if there is no beam or target polarization, the only direction the Ξ^- can be polarized is along the direction of the normal to the production plane, defined by the target, beam, and the outgoing Ξ^- (Fig. 5). For a weak decaying particle such as the $\Xi^-(1320)$, the polarization can be measured via its decaying angular distribution, which takes the form of

$$I(\theta) = A(1 - \alpha P cos(\theta)) \tag{1}$$

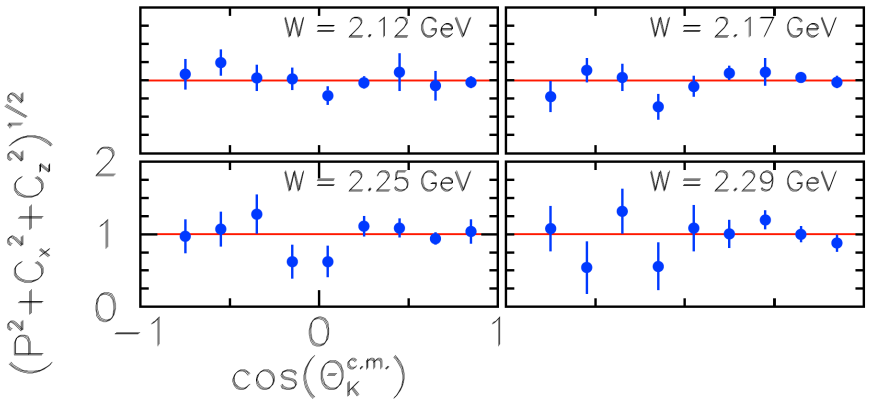

FIG. 3: The magnitude of the Λ hyperon polarization $R_\Lambda = \sqrt{P^2 + C_x^2 + C_z^2}$ is shown to be consistent with unity [14]

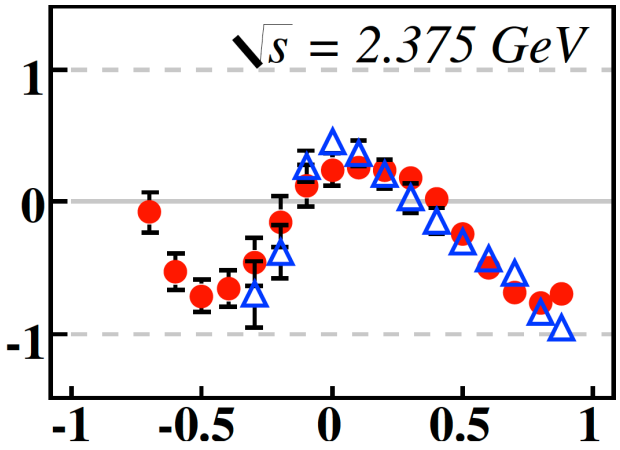

FIG. 4: The Induced Λ polarization P_Λ is shown to change signs as a function of $cos\theta^{c.m}$ [15]

For the $\Xi^-(1320)$, the value of α is -0.456, and P denotes the polarizaiton. The polarization P can be also determined by

$$P = -\frac{2}{\alpha}\frac{N^+ - N^-}{N^+ + N^-} \tag{2}$$

with N^+ denoting events in the forward direction, and N^- in the backward direction.

If there is beam or target polarization, then presumably some of the initial polarization can be transferred to the $\Xi^-(1320)$, and a measurement of the in-plane polarization of the $\Xi^-(1320)$ can become a very useful tool to probe the production mechanism of Ξ baryons. For example, recent photoproduciotn data of Λ in the reaction of $\gamma p \to K^+\Lambda$ has shown that the polarization of a circularly polarized photon beam is almost exclusively transferred to

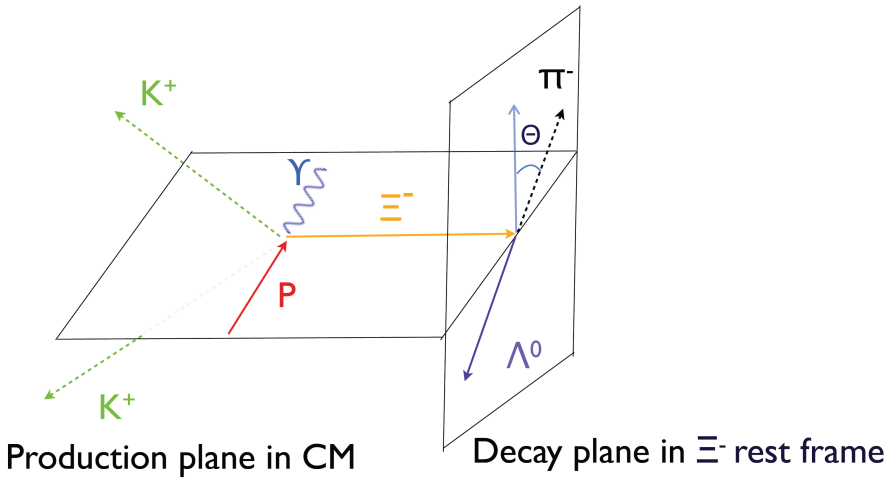

FIG. 5: Illustration of the $\Xi^- \to \Lambda\pi^-$ decay for the polarization measurement in the reaction of $\gamma p \to K^+K^+\Xi^-(1320)$. The production plane is defined by the beam, target, and the outgoing Ξ^-. The π^- angle in measure in the Ξ^- rest frame, with the z-axis for the polarization measurement defined by the normal to the production plane.

the hyperon [14]. If the production mechanism for Ξ is similar to that of the Λ, then it is not inconceivable that some of the beam polarization is transferred to the Ξ. On the other hand, in a conventional di-quark picture of baryon resonances, the polarization mechanisms of the Λ and Ξ could be fundamentally different as discussed earlier. If if is true that most of the Ξ polarization is from the valence quark contribution, then the difference between an unpolarized photon beam or otherwise, should be very small, provided that there is no target polarization.

The proposed program will the measurement of induced Ξ^- polarization, and the beam polarization transfer, since the quasi-real photon polarization could be determined on an event-by-event basis. The comparison between Λ and Ξ^- polarizations can be made, and the production mechanism can be further explored. As shown in Fig. 6, extremely clear signals of $\Xi^- \to \Lambda\pi^-$ can be identified, due to the fact that there are two narrow resonances providing kinematic constraints. If fact, such an unique feature is one of the main reason to focus on this channel, as it simplifies the analysis of the decay angular distributions greatly and makes the extraction of polarization variables much less susceptible to background contamination. As a sanity check, we used the decay angular distributions of these extremly clean sample

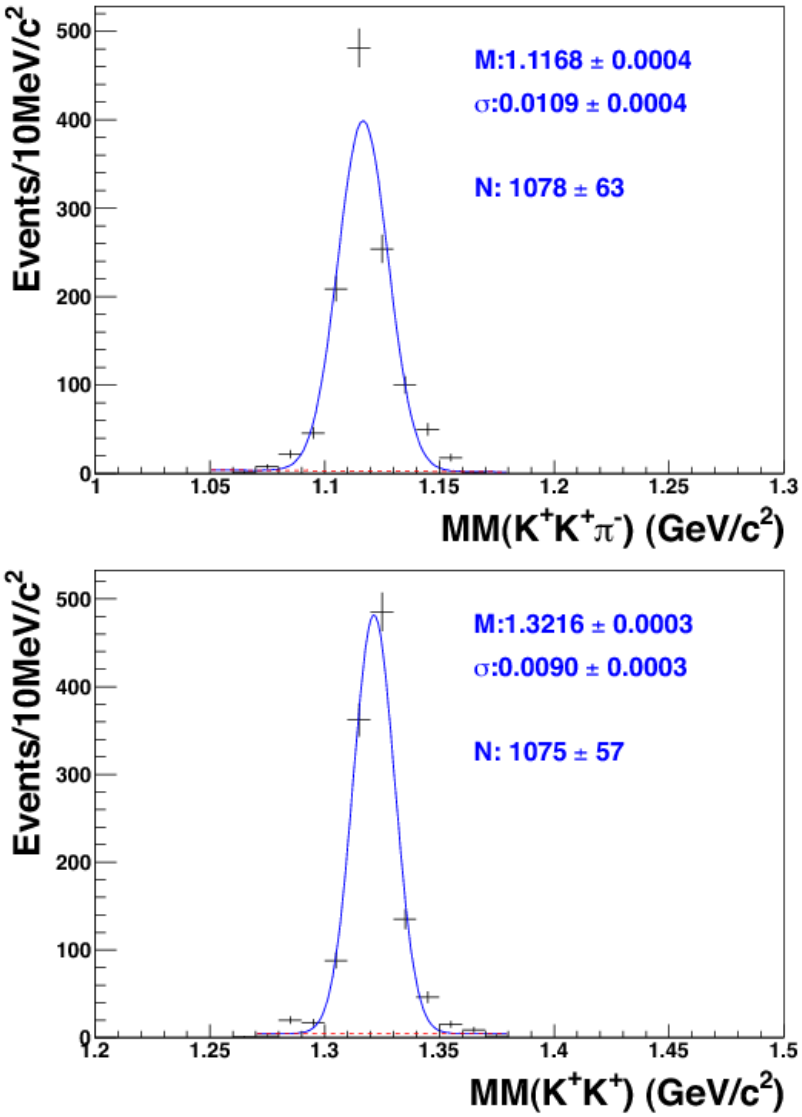

FIG. 6: Top: The missing mass spectra of the $K^+K^+\pi^-$ system off of a proton target. Events corresponding to the Ξ^- signal on the right are selected; Bottom: The missing mass spectra of the K^+K^+ system off of a proton target. Events corresponding to the Λ signal on the left are selected. The data was collected by the $g11$ [44] experiment, and the photon beam is unpolarized. The included photon energy range here is mostly from 3.0 GeV to 3.8 GeV.

of $\Xi^- \to \Lambda\pi^-$ events, and the preliminary $\Xi^-(1320)$ polarization measurement, as a function of photon energies which are shown in Fig. 7. Although the results are consistent with zero polarization, which is close to our expectation due to the fact there is no beam polarization. This result is already notably different from the induced polarization of Λ measured recently by CLAS [15]. However, it is also possible that our preliminary results are due to integrating

other kinematic variables, such as the Ξ^- angle in the center-of-mass (CM) frame.

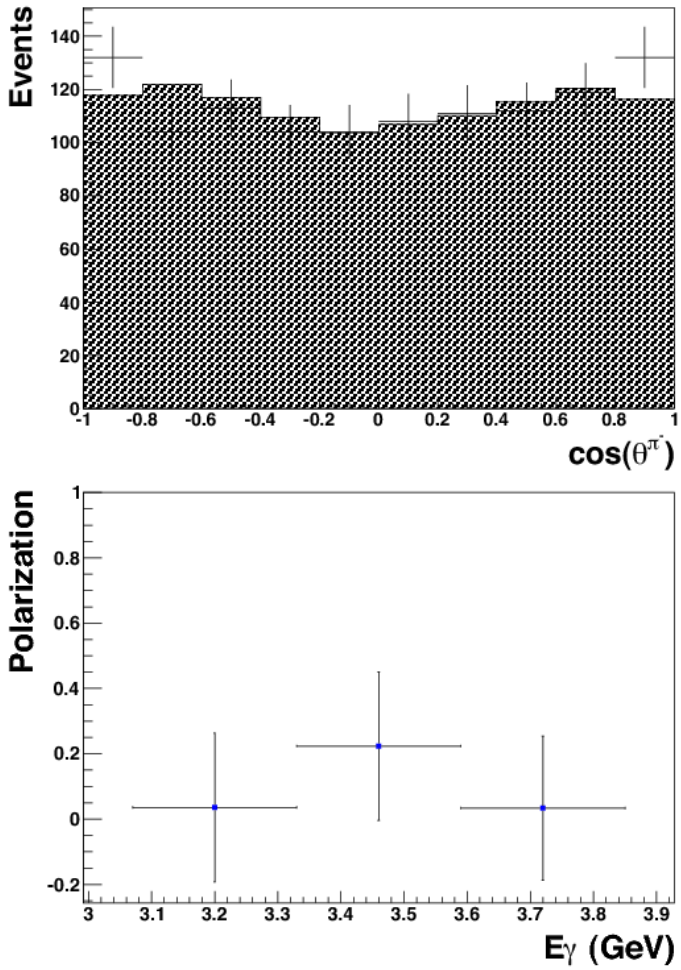

FIG. 7: Top: The integrated decay angular distribution of the Ξ^- decay. θ^π is the angle between the π^- momentum and the normal to the production plane. The shaded histogram is from simulation that is based on the differential cross sections results reported in Ref. [10]. The included photon energy range here is mostly from 3.0 GeV to 3.8 GeV; Bottom: Preliminary results of the calculated Ξ polarization out of the production plane is consistent with zero within uncertainty . Errors are statistical only. An estimated systematic uncertainty of 10% is not shown. The data was collected by the $g11$ [44] experiment, and the photon beam is unpolarized.

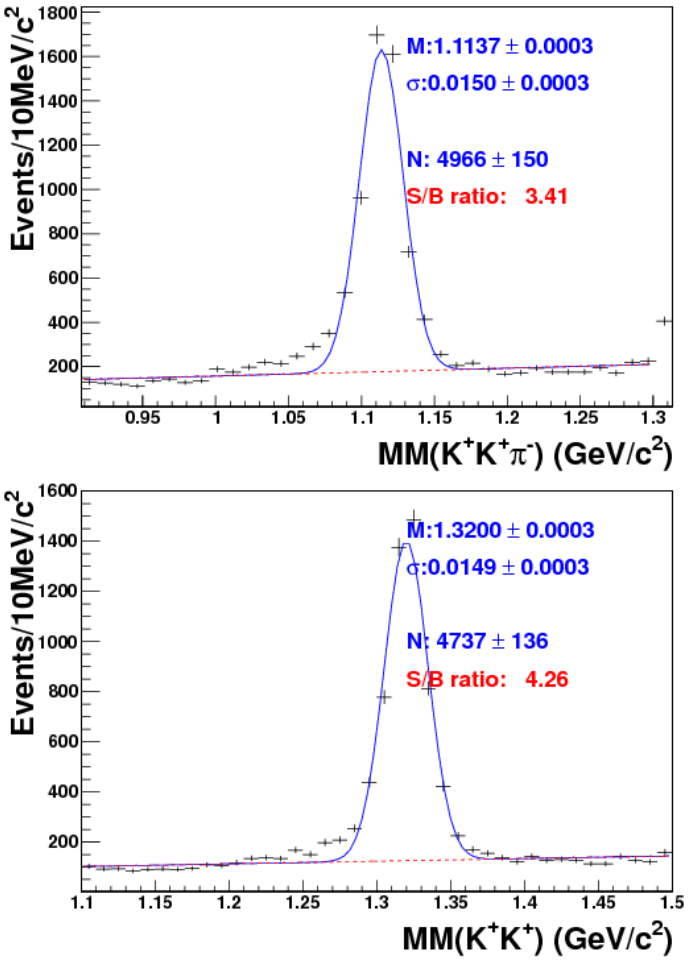

FIG. 8: Top: The missing mass spectra of the $K^+K^+\pi^-$ system off of a proton target. Events corresponding to the Ξ^- signal on the right are selected; Bottom: The missing mass spectra of the K^+K^+ system off of a proton target. Events corresponding to the Λ signal on the left are selected. The included photon energy range here is 3.3 GeV to 5.4 GeV. Only 10% of the data have been analyzed and shown here. These events are not required to have originated from within the target due to the weak decay of Ξ^-. The data was collected by the g12 experiment, and the photon beam is circularly polarized, with maximum polarization around 70% .

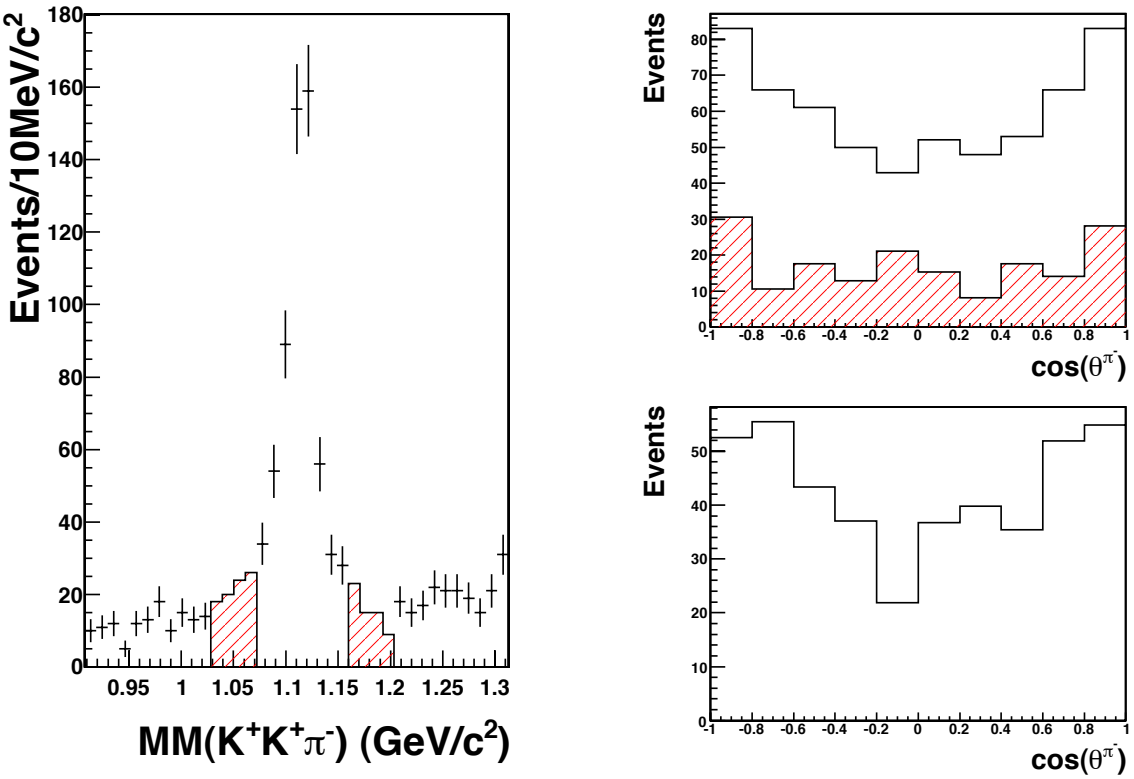

FIG. 9: Left: The missing mass spectrum of the $K^+K^+\pi^-$ system off of a proton target, from the g12 experiment. Top right: The decay angular distribution of $\Xi^- \to \Lambda\pi^-$, with the π^- being the analyzer, and the normal to the production plane defining the z-axis. The shaded events correspond to the side band events shown on the left; Bottom right: Side band subtracted of the decay angular distributions using the two histograms on the top.

III. CROSS SECTION ESTIMATION FOR THE Ω PHOTOPRODUCTION ON THE PROTON

In each of the measurements mentioned above, only a small Ω^- data sample was obtained, and the Ω-production mechanism was not well understood. Mechanism of the Ω-photoproduction should be quite specific, since it is the first baryon with constituents none of which could come from the target proton.

In the next few paragraphs, we attempt to estimate the cross section for Ω-photoproduction on a nucleon using a variety of models.

A. Vector-Meson Dominance Model

Afanasev considers Ω-production on a proton target. The photoproduction amplitude in the Vector-Meson Dominance (VMD) approximation may be written

$$f(\gamma p \to \Omega^- X)|_{VMD} = (e/f_\rho) f(\rho^0 p \to \Omega^- X) + (e/f_\omega) f(\omega p \to \Omega^- X) + (e/f_\phi) f(\phi p \to \Omega^- X), \quad (3)$$

where the photon-vector meson couplings $f_{\rho\omega\phi}$ can be obtained from the measured partial decay widths of vector mesons $\Gamma(\rho, \omega, \phi \to e^+e^-)$ [1]. In the following, we make an assumption that the leading contribution to Ω-production is due to the intrinsic strangeness component of the photon. In the constituent quark model, the ϕ-meson is primarily an $s\bar{s}$-pair, providing strange quarks in the incident photon beam. Therefore,

$$f(\gamma p \to \Omega^- X)|_{\phi MD} \sim (e/f_\phi) f(\phi p \to \Omega^- X). \quad (4)$$

Then, the photoproduction cross section is

$$f(\gamma p \to \Omega^- X)|_{\phi MD} \sim (\alpha/\alpha_\phi) \sigma(\phi p \to \Omega^- X). \quad (5)$$

Here, α is a fine structure constant, while the value $\alpha_\phi = f_\phi^2/4\pi = 14.3 \pm 0.5$ is obtained from the partial width $\Gamma(\phi \to e^+e^-) = (1.27 \pm 0.04)$ keV [1]. Using an additive quark model, we further relate cross sections of $\phi p \to \Omega^- X$, $K^- p \to \Omega^- X$, and $K^+ p \to \Omega^- X$ processes by

$$f(\phi p \to \Omega^- X) = [\sigma(K^- p \to \Omega^- X) + \sigma(K^+ p \to \Omega^- X)]/2. \quad (6)$$

Experimental data exist only for the $K^- p \to \Omega^- X$ process [7]. Using these data, we are able to estimate the photoproduction cross sections at the matching momenta, assuming

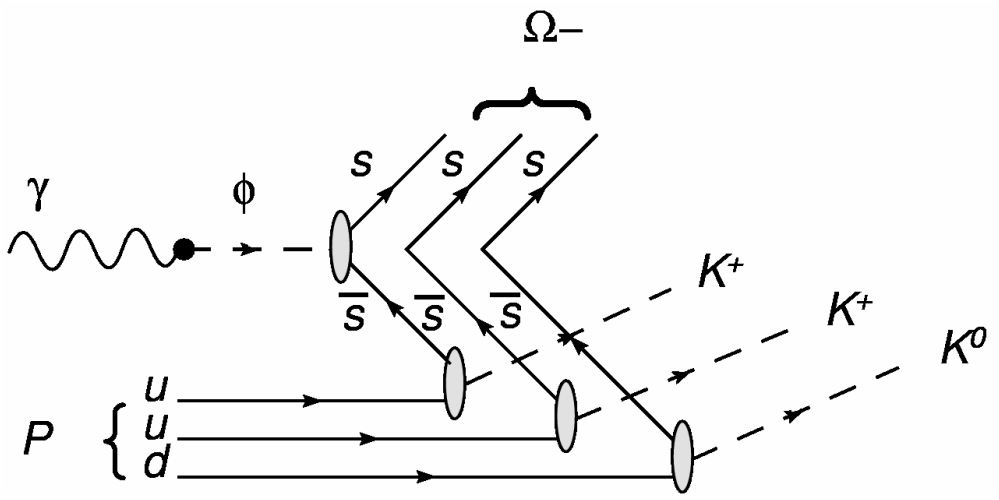

FIG. 10: Quark diagrams for the Ω-photoproduction in the VMD approach of Afanasev.

the production mechanism shown in Fig. 10. We consider the numbers obtained in this model to be upper limits. Based on this model, we estimate that, for the 11-GeV photon beam, we can anticipate Ω-baryon inclusive photoproduction cross section at the level of $\sigma_t = 0.5 - 1$ nb. Let us translate this inclusive cross section into an exclusive prediction. We estimate the exclusive cross section for $\gamma p \to \Omega KKK$ at σ_t=0.4- 0.5 nb. This follows from two independent arguments:

- Using Ref. [7] for $K^- p \to \Xi^- X$ cross section and ϕ^-VMD, we get σ_t ~40 nb for the inclusive $\gamma p \to \Xi^- X$. CLAS Collaboration gives σ_t ~15 nb for the exclusive $\gamma p \to \Xi^- KK$ at photon our previous VMD-based estimate (1 nb) by a factor of 2.5, we get the exclusive cross section of $\gamma p \to \Omega^- KKK$ as σ_t ~0.4 nb.

- Inclusive cross sections for $K^- p \to \Xi^- X$ and $K^- p \to \Omega^- X$ at 11 GeV/c appear to be in the approximate ratio 30:1 [7]. Let us assume the cross sections for $\gamma p \to \Xi^- KK$ and $\gamma p \to \Omega^- KKK$ are in the same ratio. The former is measured at CLAS to be σ_t ~15 nb [10], then the exclusive Ω cross section is a factor of 30 less, which is σ_t ~0.5 nb. Note that VMD was not used here explicitly.

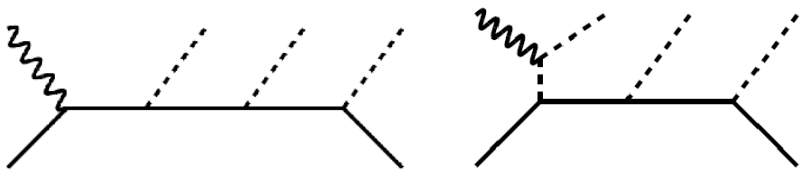

FIG. 11: Diagrams used in the calculation of the cross section for $\gamma N \to KKK\Omega$, in the phenomenological Lagrangian approach of Roberts.

B. Effective Lagrangian Model-1

The second prediction for the cross section for $\gamma N \to K^+K^+K^0\Omega^-$ is obtained by Roberts in a simple model based on a phenomenological Lagrangian. The model uses the diagrams shown in Fig. 11, where all permutations of external legs are included. This means that there are 24 diagrams like the first one, and another 18 like the second. The ground state nucleon, Λ, Σ and Ξ and two excited Ξ with $J^P = 1/2^+$ (masses of 1.91 and 2.14 GeV, respectively, taken from a quark model calculation [40]) are included in the calculation. The mesons are assumed to couple to the spin-1/2 baryons through a pseudoscalar coupling. Some of the required coupling constants are taken from a preliminary fit to CLAS data on photoproduction of the Ξ baryon. The couplings of the excited Ξs to the ground state hyperons are obtained by assuming total widths of 50 MeV and branching fractions of 30% into each of the ΛK and ΣK channels. The results from this estimate are shown in Fig. 14. The dash-dotted curve is obtained with pair of signs for the couplings of the two Ξ resonances included in the calculation. The short dashed curve is obtained when the sign of one of those couplings is flipped with the magnitude unchanged. One can expect that inclusion of other contributions may further enahnce the total cross-section for production of the Ω^-, but total cross sections are expected to be of the order of one to a few nanobarns, at most.

C. Effective Lagrangian Model-2

The third approach by Shklyar for the calculation of the Ω-photoproduction cross section (Fig. 12, which is similar to Fig. 11). The resonance production of $S = -3$ baryons can be represented by a sequence of transitions $\gamma p \to \Lambda^* \to \Xi^* \to \Omega^-$, where kaons are emitted at each step. There are three additional diagrams obtained by permutations of final kaon

momenta in the diagram depicted in Fig. 12: ($q_1 \longleftrightarrow q_3$), ($q_2 \longleftrightarrow q_3$), and ($q_2 \to q_3$, $q_3 \to q_1$, and $q_1 \to q_2$).

Here, we assume that the reaction goes through the excitation of the two heavy resonances $\Lambda^*(3000)$ and $\Xi^*(2370)$. The PDG Listings [1] indicate several heavy Λ^*- and Σ^*-states with masses close to 3 GeV. Most of their properties are unknown. Therefore, we will treat $\Lambda^*(3000)$ resonance with $J^P = 1/2^+$ as a "generic" one assuming that it corresponds to overall possible contributions from both Λ^*- and Σ^*-hyperons. The model parameters are chosen as follows: $m_{\Lambda^*(3000)} = 3$ GeV, $\Gamma_t(\Lambda^*(3000)) = 200$ MeV, Br($\Lambda^*(3000) \to$K$^*(892)$N) = 20 %, and Br($\Lambda^*(3000) \to K\Xi^*(2370)$) = 10 %. The $\Xi^*(2370)$ state is rated by two stars in the PDG Listings and has about 10 % branching decay ratio to $K\Omega^-$ and 20 % decay fraction to the "generic" K$^*(892)\Lambda$ and K$^*(892)\Sigma$ final state. The spin and parity of $\Xi^*(2370)$ are also unknown and calculations are also done assuming $J^P = 1/2^+$. The total width of $\Gamma_t(\Xi^*(2370)) = 80$ MeV which is taken from PDG [1]. The interaction Lagrangian is chosen as

$$
\begin{aligned}
L = {} & g_{\Omega\Xi^*K}\left[\bar{\Omega}(x) i\gamma_5 \Xi^{(*)}(x)\right] K(x) \\
& + g_{\Lambda^*\Xi^*K}\left[\bar{\Xi}^{(*)}(x) i\gamma_5 \Lambda^{(*)}(x)\right] K(x) \\
& + g_{\Lambda^*K^*N}\left[\bar{N}(x)\sigma_{\mu\nu}\Lambda^{(*)}(x)\right] K^{(*)\mu\nu}(x) \\
& + \frac{e\, g_{K^*K\gamma}}{4m_K}\epsilon_{\mu\nu\rho\sigma} K^{(*)\mu\nu}(x) F^{\rho\sigma}(x) K(x) \\
& + \text{h.c.},
\end{aligned}
\tag{7}
$$

where isospin indices are omitted. The coupling constants are calculated from the corresponding decay branching ratios. The $K\Xi^*\Lambda^*$ and $K\Xi^*\Omega$ vertices are dressed by the form factor

$$
F_s(q^2) = \frac{\Lambda_s^4}{\Lambda_s^4 + (q_s - m_R^2)^2}, \tag{8}
$$

where q_s is a momentum of the propagating baryon in the s-channel and m_R is a mass of the resonance. The formfactor used at the $t-$channel vertex has the form

$$
F_t(q^2) = \frac{\Lambda_t^4 + m_{K^*}^4}{\Lambda_t^4 + (t + m_{K^*}^2)^2}, \tag{9}
$$

where $t = (q_1 - k)^2$ for the diagram depicted in Fig. 12. The cutoff parameter is chosen to be $\Lambda_s = \Lambda_t = 1.5$ GeV.

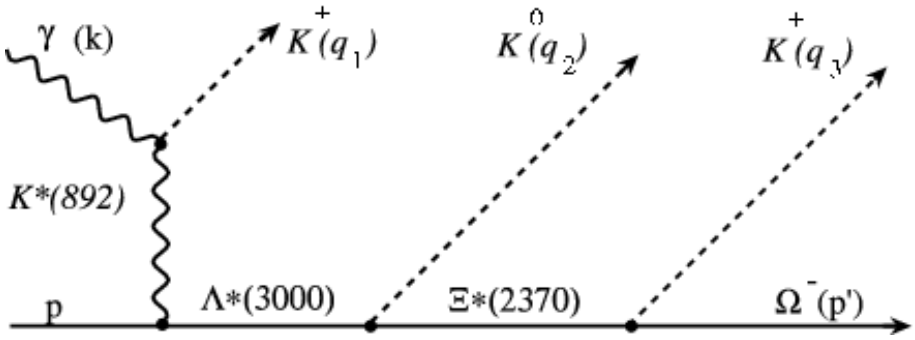

FIG. 12: Feynamn diagram for the $\gamma p \to K^+K^0K^+\Omega^-$ transition in the effective Lagrangian approach of Shklyar.

Having resonance production mechanism, the exclusive $\gamma p \to K^+K^0K^+\Omega^-$ cross section is estimated to be about 0.5 nb at $E_\gamma = 11$ GeV. This is a conservative estimation and inclusion of additional channels would lead to a larger total cross section. The measurements of the invariant mass distributions can provide an important information on the Ω^- production process. The invariant mass distribution $\frac{d\sigma}{dM^2_{q_3,p_\Omega}}$ calculated in the case at hand is shown in Fig. 13. Here the notation $M^2_{q_3,p_\Omega} = (q_3 + p_\Omega)^2$ is adopted, where q_3 is a kaon momentum. Due to symmetrization the charge kaons can be emitted at any vertex which corresponds to the different kinematical situations. The interplay between contributions where the charge kaons are emitted at $\Lambda^*\Xi^*K$ and $\Xi^*\Omega^-K$ vertices leads to the broad structure in the M_{q_3,p_Ω}= 2.2...2.6 GeV invariant mass region with the deep around $\Xi^*(2370)$ resonance mass. The second peak at 2.9 GeV is due to the $\Lambda^*(3000)$ excitation. Hence, the invariant mass distribution could shed light on the details of the Ω^- production mechanism and distinguish between resonance and resonance contributions.

D. Summary

Overall, Fig. 14 shows the cross section estimation as obtained for the Ω^- photoproduction on the proton. Near the threshold, the cross section is small, as expected, but quickly grows into the nanobarns range (or tens of nanobarns, depending on the coupling constants). A cross section of a few nanobarns in the energy range of interest seems to be a safe bet. The critical feature is that all four estimations are consistent with each other. The numbers are an indication of what one can expect. Clearly, we shouldn't believe them (effective

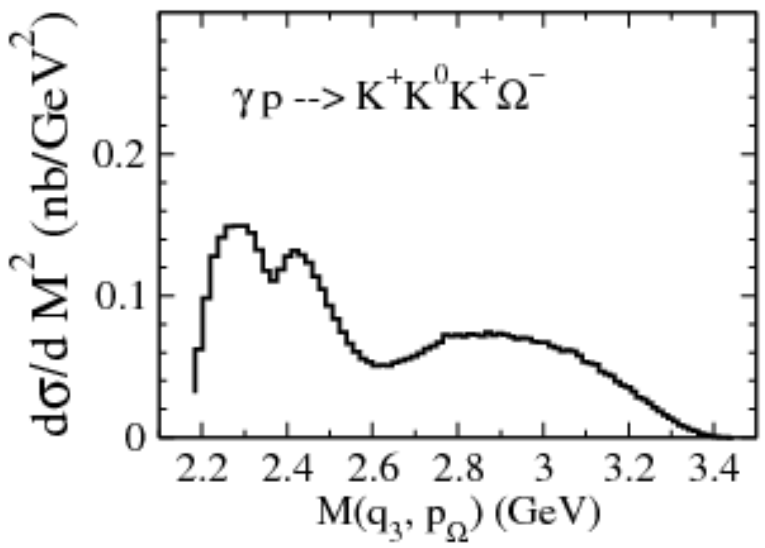

FIG. 13: Invariant mass distribution for the resonance production mechanism shown in Fig. 12.

Lagrangian approach) very far from threshold, as the cross sections continue to rise but we have no idea how strongly energy dependent to make those.

One can estimate [16] that the photoproduction rate for $\gamma p \to \Omega^- X$ is simply α/π times the measured hadroproduction rate at ANL [6], which agreed with the above estimations. The angular distribution of the inclusive and exclusive events may provide a clue for the Ω^- production mechanism. For example, whether production of $\Omega(sss)$ is enhanced at small t or small u [16].

Brodsky's estimations addressed to one approach to $\Omega(sss)X$ [16]. That is to consider $g \to s\bar{s}$ the origin of one of the s-quarks. This produces the minimum number of final-state quarks. The other two strange quarks can be made either by gluon splitting $g \to s\bar{s}$ or by double intrinsic strangeness $|uuds\bar{s}\bar{s}>$ Fock state of the proton. The gluonic intermediate states should be minimized [17]. The $gs\bar{s}$ vertex produces one of the needed strange quarks. The intrinsic strangeness mechanism does not need explicit gluons. One can create the strange quark pairs within the hadron wave function via QCD Coulomb exchange. This gives the $|uuds\bar{s}s\bar{s}>$ Fock state amplitude. This process is maximally efficient at threshold. The analogous $|uud\bar{c}c\bar{c}>$ double intrinsic charm Fock state can account for the extraordinary $\pi N \to J/\psi J/\psi X$ events seen by the NA3 Collaboration [18] as has been discussed in Ref. [19]. All of the double J/ψ events are made at high $x_F(total) > 0.4$.

Additionally, Shklyar estimated the $\gamma p \to \Omega\bar{\Omega}p$ cross section production. Unfortunately,

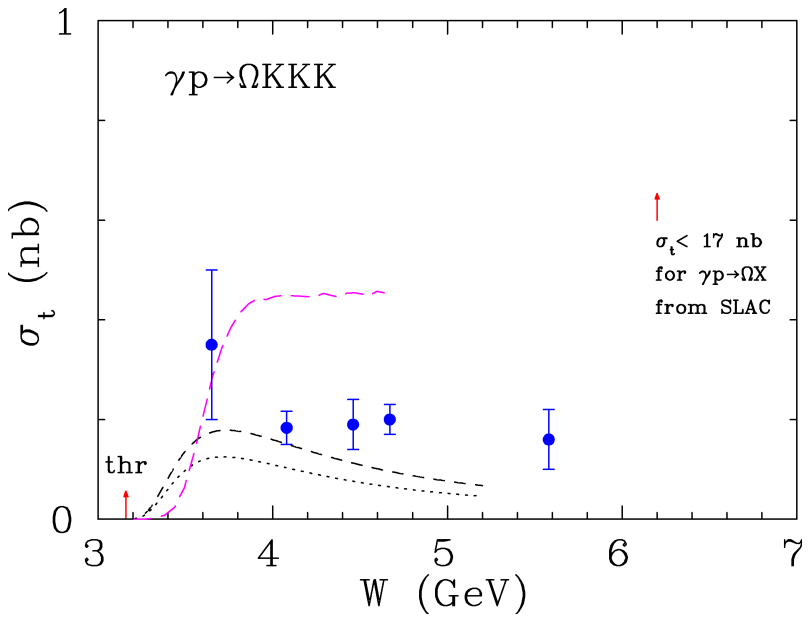

FIG. 14: Total exclusive cross section for the Ω-photoproduction. Blue filled circles show the conservative phenomenological translation of the hadronic cross sections into the photoproduction ones. Dash-dotted (short dashed) curve show phenomenological Lagrangian-1 calculations (see text for details). The dotted curve presents the Ω-production using a different Lagrangian-2 approach. The red arrow indicates the threshold which is W = 3.16 GeV (E_γ = 4.85 GeV).

the estimated total production cross section is too small – picobarns or smaller. It would be hard to use this channel for any reliable analysis.

E. ΩN and ΞN Elastic Scattering

The fact that all ground-state hyperons decay weakly allows one to consider the possibility that they can interact with a second proton in the target. This secondary interaction takes place via the strong interaction, and therefore may occur often enough to observe with the CLAS detector. $SU(3)_F$ symmetry dictates that the cross section for hyperon-nucleon scattering should be comparable to that of NN scattering; a simple model [36] gives the relation

$$\sigma(\Xi^- p) + \sigma(pp) = 2\sigma(\Lambda p)$$

which makes it possible to estimate the event rates we can expect in an experiment with CLAS12.

A detailed study of the interaction of the Ξ hyperons with the nucleon may help to illuminate $SU(3)_F$ symmetry breaking in the baryon-baryon interaction. A particular process, $\Xi^- p \to \Lambda\Lambda$ may point to the existence of the H dibaryon, which has not yet been observed,[38, 39] or allow the first direct measurement of the parity of the ground-state Ξ^-.[35]

The existing data on hyperon-nucleon scattering is sparse for $S > 1$, consisting primarily of a few events seen in high-energy bubble-chamber experiments done in the 1970s.[26–29] Recently, a new measurement at lower energies was attempted using a scintillating fiber target.[25] Out of more than six thousand Ξ^- events seen in the $p(K^-, K^+)\Xi^-$ process, a single candidate event for the elastic scattering process $\Xi^- p \to \Xi^- p$ remained, leading to an upper limit of 28 mb. Quality data on $\Xi^- p$ scattering would help to constrain theoretical models for this process and help to illuminate the nature of the hyperon-nucleon interaction.[30–34]

Ref. [22].

IV. CROSS SECTION ESTIMATION FOR THE Ξ PHOTOPRODUCTION ON THE PROTON

There are several theoretical attemts to calculate excited Ξ states using effective Lagrangian approach.

... **Winston, Helmut&Kanzo** ...

V. EXPERIMENT WITH CLAS12 FOR THE Ω- AND Ξ-BARYONS

A. Very Strange Photoproduction Experiment

The Ω^- has never been observed in photoproduction experiments due mainly to its very small production cross section. Excited Cascade states also have cross sections of the order of a nb. It is clear, therefore, that any experiment wishing to measure these reactions must combine high luminosity with a large particle acceptance and a beam energy extending well above threshold. Such a scenario will be realised with the CLAS12 detector system after

the JLAB upgrade, making photoproduction measurements feasible for the first time.

To estimate the number of Ω^- and cascades produced we take the nominal CLAS12 luminosity of $10^{32}\text{cm}^2\text{s}^{-1}$. We consider 3 possibilities for the production photon in the energy range 5–11 GeV; (a) a real bremsstrahlung photon from the e^- beam in the liquid hydrogen target, (b) a quasi-real photon tagged in the forward tagger (FT), and (c) an untagged quasi-real photon, i.e. the low angle scattered e^- not in the FT acceptance. Cases (a) and (c) will be experimentally indistinguishable.

The flux of real bremsstrahlung photons has been estimated using two methods; first through evaluating Eq. (27.28) in the PDG book, giving the number of photons per electron,

$$n_\gamma = \frac{d}{X_0}\left[\frac{4}{3}\ln\left(\frac{k_{max}}{k_{min}}\right) - \frac{4\,(k_{max}-k_{min})}{3E} + \frac{k_{max}^2 - k_{min}^2}{2E^2}\right]$$

with $d = L\rho$=5 cm $\times$ 0.0708 gcm^{-3}. $X_0 = 63$ is estimated from two different PDG Eqs, (27.22) and (27.24). So for $k_{max} = 11$ GeV and $k_{min} = 5$ GeV, n_γ =0.0040. The second method used a GEANT4 simulation of 11 GeV e^- incident on a 5 cm of liquid hydrogen. The number of photons leaving the target per e^- was found to be 0.0048, in reasonable agreement with the calculation. Production estimates for this case will use the lower calculated figure of 0.0040. To calculate the photon luminosity we take $L_\gamma = L_e \times \frac{n_\gamma}{2} = 2 \times 10^{32} cm^2 s^{-1}$, where the factor 2 on the denominator accounts for an effective target length, half the length of the target cell.

The flux of tagged and untagged quasi-real photons has been calculated via the RADGEN1.0 programme [41], which accounts for internal radiative corrections to the cross section. For both cases the scattered electron energy is integrated from 0.5 to 6 GeV. While for the tagged case the scattered angle is integrated from 2.5 to 4.5°. The resulting luminosities are $L_{\gamma * tag} = 8.7 \times 10^{31} cm^2 s^{-1}$ for tagged and $L_{\gamma * unt} = 3.2 \times 10^{32} cm^2 s^{-1}$ for untagged.

We therefore expect that most baryons will be produced by untagged quasi-real photons with a further 63% from untagged bremsstrahlung and 27% from tagged quasi-real photons. Baryons from the two former mechanisms will have to be fully reconstructed with any associated particles to fully determine the reaction. On the other hand, with tagged quasi-real photons, it is possible to measure incomplete final states and use the missing mass to determine the reaction. Using such a method can substantially increase the reaction acceptance.

B. Mesurements of Ω^- production

The primary goal of the Ω^- programme is to measure the photoproduction cross section which is sensitive to the production mechanism. We start with a high luminosity beam and low cross section reaction and so to investigate the feasability of such measurements we have analysed the products from this reaction, having being passed through the CLAS12 parameterized Monte Carlo simulation FASTMC.

C. Measuring the Ω^- final state

The relevent production and decay chain for Ω^- production is,

$$\begin{aligned}
\gamma p &\rightarrow K^+K^+K^0\Omega^- \\
K^0 &\rightarrow \pi^+\pi^- \quad (BR = 34\%) \\
\Omega^- &\rightarrow K^-\Lambda \quad (BR = 68\%) \\
&\rightarrow \pi^-\Xi^0(\pi^0\Lambda) \quad (BR = 24\%) \\
\Lambda &\rightarrow p\pi^- \quad (BR = 64\%)
\end{aligned}$$

To fully measure the final state requires detection of 7 particles; $2K^+$, π^+, π^- from K^0 decay, K^- from Ω^- decay and the proton and π^- from the Λ decay. If the production photon is tagged then in principle it is possible to identify the Ω^- events through measuring the 3 associated kaons (with the $\pi^+\pi^-$ for the K^0), this is then sufficent to fully reconstruct the production reaction. Further measurement of the Ω^-, K^- or π^-, allows reconstruction of the Ω^- decay and provides a means of background rejection.

In addition to the standard FASTMC reconstruction an additional constraint has been placed on the vertex position of the measured particles. Many of the intermediate particles can travel significant distances in the detector before decaying and so some particles may be created outside of the vertex detector. It is assumed for this analysis that such particles will not be reconstructed. This is erring on the side of caution as in reality such particles can be reconstructed, all be it with degraded momentum resolution. A particle was considered to be detected inside the vertex detector if its vertex distance from the centre of the target was less than 5 cm transverse and 19cm longitudinal. Such a constraint results in the reconstruction loss of 10% K^-, 23% K^0 and 50% of Λ particles. These losses are accounted for in the event

rate estimates in Table 4.

It was found that the π^- from the Λ decay suffered from particularly poor acceptance, due to it having low momentum, forward angle and an inward bend. This subsequently leads to a poor acceptance for the detection of all 7 particles in the final state.

We consider four different final state topologies; (i) Detect $2K^+$, π^+, π^-, (ii) as (i) plus K^-, and cut on reconstructed mass of Λ, (iii) as (i) plus π^- and cut on reconstructed mass of Ξ^0, and (iv) detect all 7 final state particles from $K^-\Lambda$ decay. The production acceptances are shown in Figure 15 as a function of beam energy.

The additional kinematic and vertex cuts placed during the analysis were: (i) for K^0 detection the π^+ and π^- were required to have the same vertex and reconstruct the mass of the K^0 within 4σ, (20 MeV); (ii) for the case of a missing Λ, the missing mass had to be within 4σ, (120 MeV) of the Λ mass; the K^- vertex position had to be greater than 2 mm from the K^+ vertex, and (iii) For the missing Ξ^0 a 3σ cut was placed on the missing mass and the π^- vertex had to be greater than 2 mm from the K^+ vertex.

D. Event rates for Ω^- photoproduction

We can now calculate the expected event rates for these four possible measurements. We assume a photoproduction cross section of 0.3 nb, from Fig. 14, a tagged luminosity of $8.7 \times 10^{31} cm^2 s^{-1}$, and untagged $5.2 \times 10^{32} cm^2 s^{-1}$. Table 4 shows the detection efficiencies, production rates and measured events per hour for the CLAS12 detector, operating at half toroidal field strength, with an electron beam luminosity of $10^{32} cm^2 s^{-1}$.

The highest possible event rate will come from detecting the 3 associated kaons, an electron in the Forward Tagger and reconstructing the Ω^-. In 119 days of beamtime, this would provide 10k Ω^- integrated over all energies and angles.

Estimates of background processes, outlined in Sec.V E, are very high for this 3K topology (approximately 1:10, signal to background). In this case detecting part of the Ω^- decay in addition appears to be the more appealing method. We can measure either the K^- or the π^- from decays to ΛK^- and $\Xi^0\pi^-$ respectively. The latter has a more uniform acceptance over all beam energies, whereas the former has a higher overall efficiency as shown in Fig. 15. We estimate, in 119 days, we will obtain 1.4K and 1.1K events for the additional K^- and π^-. This would provide around 100 events per 250 MeV photon beam energy bin.

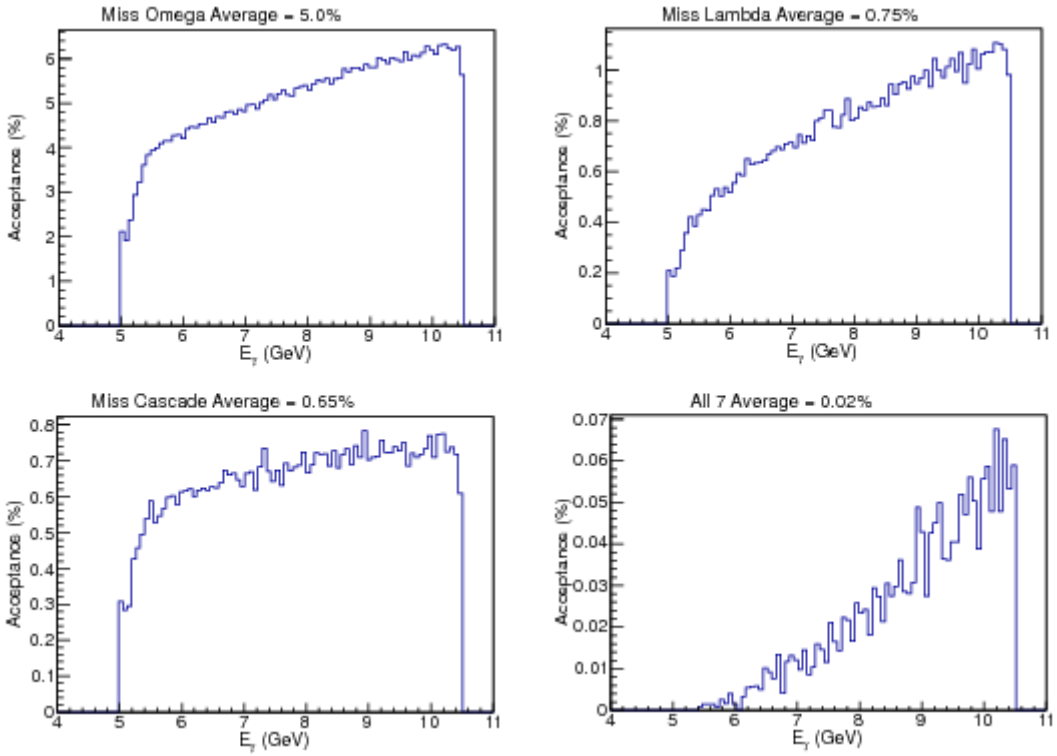

FIG. 15: The acceptance for phase space Ω^- detection as a function of photon beam energy. Top left recquires detection of $2K^+$, π^+, π^-; top right, an additional K^-; bottom left, an additional π^- from Ω^- decay to $\Xi^0\pi^-$; and bottom right detection of all 7 charged particles in Ω^- to $K^-\Lambda$ channel.

Detected	Det. Eff. (%)	Vertex Eff.	Prod. Rate (1/h)	Measured Events (1/h)
$K^+K^+K^0$	5.0	77	94	3.6
$K^+K^+K^0K^-$	0.75	70	94	0.5
$K^+K^+K^0\pi^-(\Xi^0)$	0.65	70	94	0.4
All 7	0.02	35	561	0.04

TABLE IV: Event rate estimates for 4 different scenarios. Measured events is the product of the detection efficiency, vertex efficiency and produciton rate.

Detecting the full final state will lead to only around 100 events in total but will provide a useful systematic check of the acceptances.

E. Background

In principle, measuring a final state with a relatively low cross section and large multiplicity in the final state is a daunting task as large backgrounds from other physics processes can overwhelm the signal of interest. However, Ω^- photoproduction has a number of signatures which can help reduce the hadronic background; it is produced in association with 3 kaons, it has a decay vertex detached from the production vertex and there is a further detached vertex and strange particles after its decay. To estimate the backgrounds contributing the the various final states an event generator based on Pythia was used [42]. The hadronic background produced was then normalised to the expected cross section for Ω^- photoproduction of 3 nb. As the number of hadronic events produced over 100 days is of the order 10^{11} the resulting histograms from 2×10^8 simulated events had to be scaled up significantly.

The results for when just the 3 kaons are detected are shown in Fig. 16. We see a considerable background is expected in this case and integrating over the peak region the signal to background ratio is around 1:10. It may be possible to significantly reduce this background by investigating other detected particles, but this has not been attempted at this stage.

If we now require a K^- in coincidence the situation is improved. First cutting on the missing mass around the Λ reduces the signal to background ratio to around 1:2. In addition, if a cut on the vertex difference of the K^- and K^+ of greater than 2 mm is apllied (expected resolution is around 0.5 mm) then zero background events survive, giving a super clean signal, see Fig. 17 left plot. A similar situation is found for the decay detecting an additional π^- from the decay to $\Xi^0\pi^-$, although in this case it appears the final background may not be zero, it is however expected to be lower than the signal.

F. Determination of the Spin-Parity of the Excited Cascades

However, the limitation of beam energy makes the sighting of missing cascade resonances at higher mass less likely. Even if we do observe some of these higher states, it is unlikely that there will be enough statistics and the spin parity measurement could be performed.

In order to determine Spin and Parity of an excited cascade, a very useful tool, so called double moment analysis (DMA) can be deployed [21, 23]. If only the reaction of $\Xi^{*-} \rightarrow$

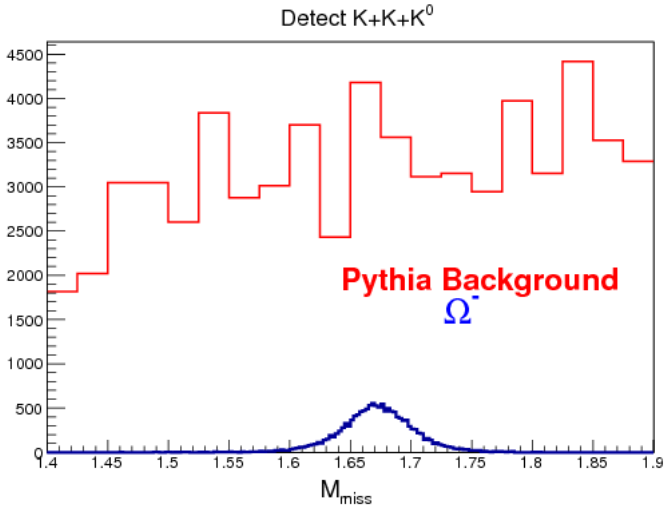

FIG. 16: The expected event distrbution for Ω^- photoproduction, blue, and Pythia background, red.

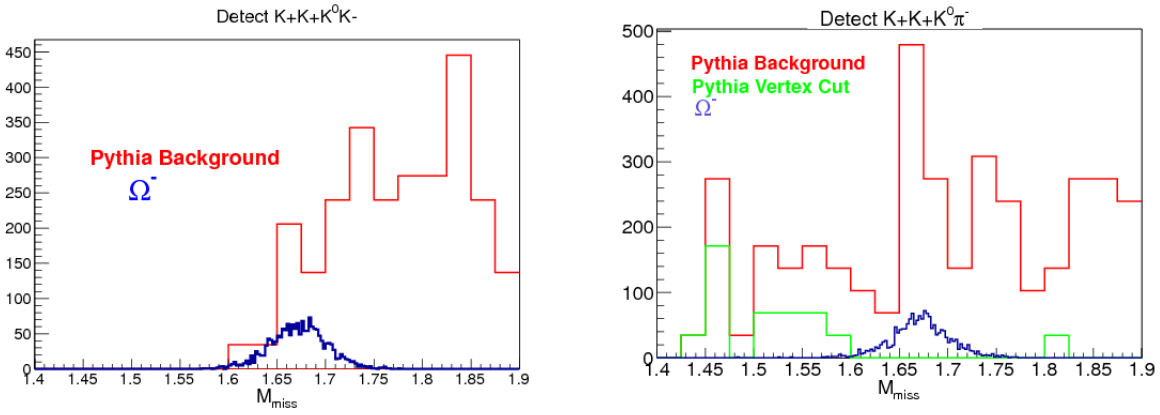

FIG. 17: The expected event distrbution for Ω^- photoproduction, blue, Pythia background, red, and Pythia background with a vertex cut, green. Note, in the left plot the vertex cut removes all Pythia background and so its entries are zero.

$\Lambda(\frac{1}{2})+\pi^-(0^-)$ is reconstructed, then due to the Minami ambiguity, there could be two solutions of $J^{\pm P}$. In order to solve the problem, one needs to detect the decay of the daughter hyperon as well, for example, $\Lambda \to p\pi^-$. If there are sufficient statistics, then the double moments can be analyzed to determine the J^P assignment of the parent cascade. The double moments, typically noted by $H(lmLM)$, is defined by:

$$H(lmLM) = \Sigma D^L_{Mm}(\theta_1, \phi_1) D^l_{m0}(\theta_2, \phi_2) \tag{10}$$

with the θ_1, ϕ_1 being the decay angles of Ξ^*, and θ_2, ϕ_2 being the decay angles of Λ. The DMA technique takes advantage of the fact there is linear dependence between different double moments, given by

$$H(11LM) = P(-1)^{J+\frac{1}{2}} \frac{2J+1}{\sqrt{2L(L+1}} H(10LM) \tag{11}$$

This linear dependence gives simple, and multiple tests for J^P assignment, for multiple combinations of any odd $L \leq 2J$ and $M \leq L$, therefore providing reliable measurement of the quantum numbers of the excited cascades. In fact, this is how the J^P of the $\Xi(1820)$ state was determined, needing only 50 signal events [21]. In order to perform such analysis, it is necessary to reconstruct the whole decay chain of Ξ^*, such as $\Xi^{*-} \to \Lambda\pi^-$, $\Lambda \to p\pi^-$.

The typical efficiency for detecting the proton from the Λ decay is around 50% at CLAS, and expected to be similar at CLAS12. Taking into account that Λ decays to $p\pi^-$ only 64% of the time, the number of excited cascade events, which can have the decay chain reconstructed, will shrink by a factor of three, when compared the requirement for identifying them from invariant mass spectra such as $\Lambda\bar{K}$, which does not need to reconstruct the decay of Λ. The implication is that, in order to measure the J^P of excited cascades, one need to conduct the experiment at as high energies as possible, in order to reach the region where the cross section is sizable, to compensate the inefficiency of detecting multiple final state particles.

Our conservative estimate, using the projected CLAS12 luminosity, would require roughly 3 months beam time using a quasi-real photon beam, to confirm the spin-parity assignment of $\Xi(1820)$) with at least an order of magnitude more than any previous data. This estimate was made with the assumption that at E_γ above 6 GeV, the $\Xi(1820)$ cross section would be comparable with of $\Xi(1530)$ near 4 GeV [10]. Data on other higher mass states would almost certainly amount to discoveries.

G. MC for the Direct Tracking Reconstruction

H. Forward Tagger

In this section we outline the forward tagger (FT) equipment which will characterise and identify quasi-real photons via measurement of electrons scattered at small-angles. The FT

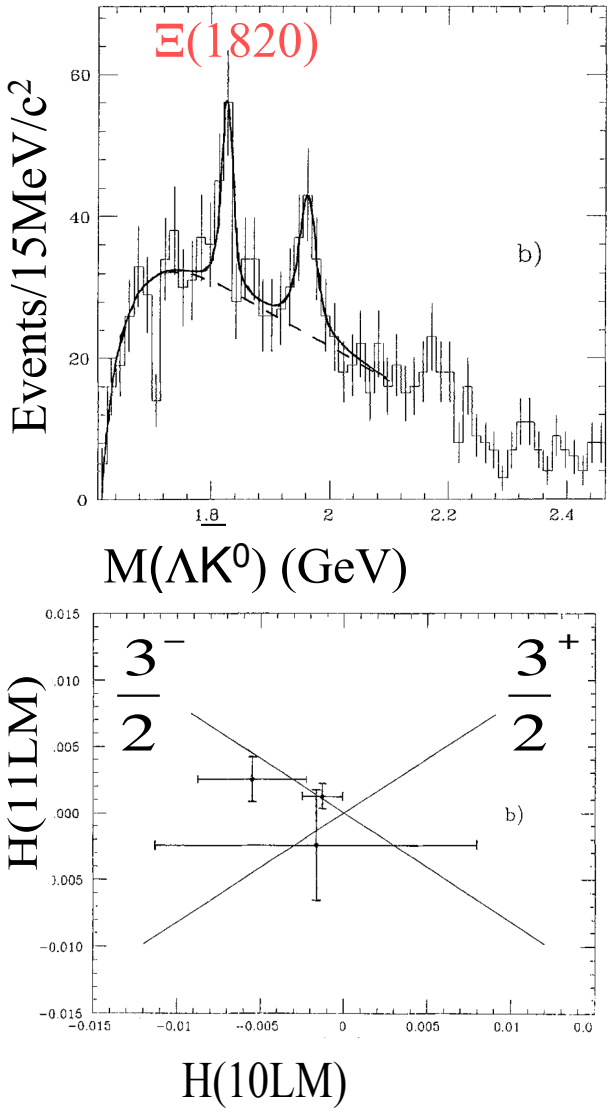

FIG. 18: Top: Invariant mass spectrum of $\Lambda\bar{K}^0$, in the inclusive $\Xi - Be$ reaction [21]; Bottom: The $H(11LM)$ moment vs the $H(10LM)$ moment for the $\Xi(1820)$ signal region

will provide electron detection for the region $2.5^\circ < \theta_{e'} < 4.5^\circ$ outside of the acceptance region of the CLAS12 detector. The FT comprises a *calorimeter* (FT-CAL), to identify the scattered electron, measure the electromagnetic shower energy and provide a fast trigger signal. A *tracker* (FT-Trck), will provide accurate measurement of the scattering angles ($\theta_{e'}$ and $\phi_{e'}$) and a *scintillation hodoscope* (FT-Hodo) will provide high efficiency e/γ separation. A dedicated trigger system will provide a fast signal to identify a timing coincidence with

signals from CLAS12.

The three components of the FT will be placed between the High Threshold Cerenkov Counter (HTCC) and the torus support, at about 190 cm downstream of the target (nominal) position. Figure 19 shows a CAD drawing of the FT elements integrated in CLAS12.

I. The calorimeter: FT-CAL

The geometrical size of the calorimeter is determined by the need for coverage in close proximity to the beam line (2.5° corresponds to ~ 8 cm) and the limited space available in this region (at most ~ 40 cm along the beam axis). This requires a compact calorimeter with a small radiation length. The size of each calorimeter pixel should be comparable with the characteristic transverse size of the electromagnetic shower or Moliere radius to contain the signal induced by incident electrons to few pixels, thus minimizing pixel rates and pile-up. FT-Cal will be based on homogeneous $PbWO_4$crystals, arranged in an array of 408 crystals of size 15×15×200 mm^3. In recent years materials such as $PbWO_4$ have been extensively studied and shown to be very resistant to radiation damage, which can be significant in this forward angle region close to the beamline. The $PbWO_4$ has a very fast scintillation decay time (6.5 ns), a very small radiation length (0.9 cm) and small Moliere radius (2.1 cm). With this design an energy resolution of $(2\%/\sqrt{E(GeV)} \oplus 1\%)$ is expected. The electron energy resolution is a crucial factor to determine precisely the photon energy and ensure the exclusivity of the measured reaction via missing mass techniques. However, since we are interested in low energy electrons and high energy photons, the energy resolution on the latter will be significantly better than the resolution on the electron.

J. The scintillation hodoscope: FT-Hodo

The primary aim of the hodoscope for the forward tagger is to discriminate between photons and electrons that produce an electromagnetic shower in the calorimeter. The scintillation hodoscope, placed in front of the calorimeter, will be made of 2 layers of Eljen EJ-204 plastic scintillator tiles read-out by Hamamtsu 3×3 mm^2 silicon photomultipliers (S10362-11-100C) via ∼4 wavelength shifting fibers per hodoscope tile. Each hodoscope plane will be segmented into around 120 elements, most of which have a pixel size corre-

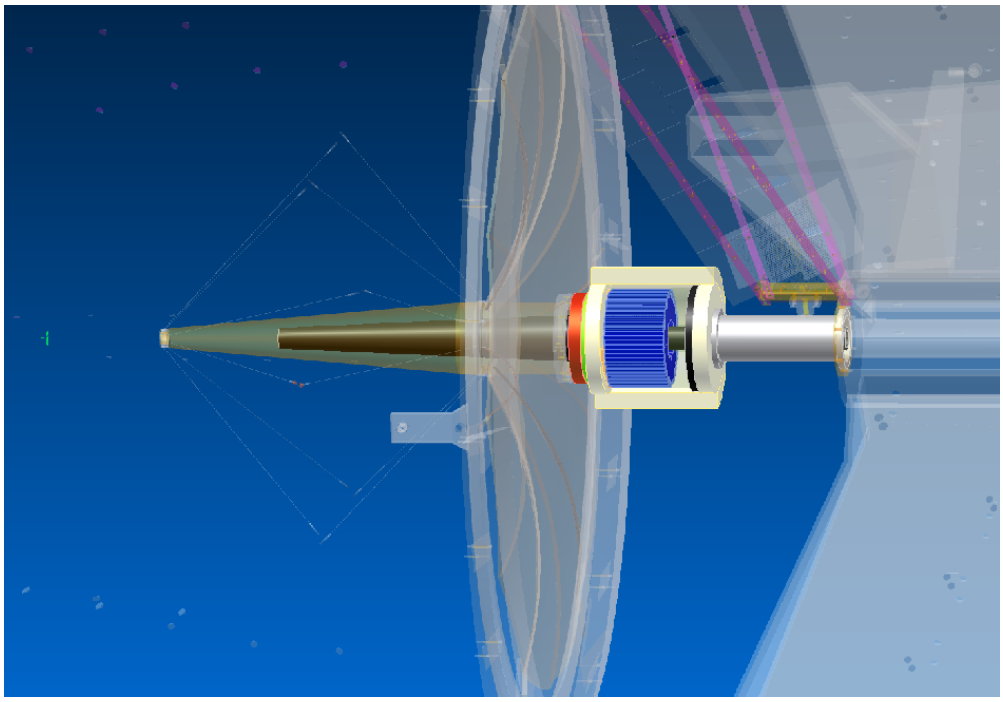

FIG. 19: CAD drawing showing the integration of the FT in CLAS12. The FT is located in the free space between the HTCC and the first DC layer. The calorimeter (FT-CAL) shown in blue is located at about 190 cm from the interaction point, shown by the green cross, and is enclosed in a Rohacell case to provide thermal insulation. FT-HODO (green) and first tracker layer of FT-TRAC (red) are located in front of the calorimeter. A tungsten cone in black shield the FT from Møller electrons and electromagnetic background created by the beam.

sponding to 4 calorimeter crystals. The inner ring comprises tiles having dimension of a single calorimeter crystal. The double layer design of FT-Hodo reduces to less than 1% hits from the splashback of charged particles from the calorimeter from incident photons, which otherwise could result in particle misidentfication due to the false firing hodoscope elements. The hodoscope layers comprise 7 mm and 15 mm thick scintillator tiles, with the latter layer designed to give sub nanosecond timing resolution for the particle. The requirement of a coincident hit between the layers will also reduce contributions of false events from SiPMT noise. The wavelength shifting fibres will be fusion spliced to optical fibre having $\sim$ 15 m attenuation length. The fibres will connect to the SiPMTs away from CLAS12 in a radiation safe region.

K. FT-TRAC

The role of the tracker is to provide a reconstruction of the track of charged particles, essentially electrons, with polar angles between 2.5° and 4.5°. In these forward angle regions the background count rate can be several hundreds of kHz/mm^2 requiring a highly segmented high rate tracking system. FT-Trck will comprise two double layers of Micromegas detectors located in the space between the calorimeter and the High Threshold Cherenkov Counter (HTCC). The detectors will be annular-shaped with inner and outer radii of 65 mm and 160 mm respectively. The use of two micromegas layers is a compromise to achieve an efficient background rejection and track reconstruction with a low material budget. These two layers are each composed of two single Micromegas with perpendicular strips, enabling the (X,Y) coordinates of a track to be determined. The pitch is 500 μm, which leads to a spatial resolution better than $500/\sqrt{12} = 144\ \mu m$. Angular resolutions for electrons of $\sim$ 1.7% and 2.8° in θ and ϕ are expected.

The FT readout will follow the scheme adopted for the Micromegas based central tracker detectors. The frontend electronics will provide pre-amplification and shaping of the detector signals, pipeline buffering during the trigger generation process, digitization and compression of selected event data. This is then delivered to the backend electronics which will pack the data and interface with the CLAS12 event building system. The readout comprises about 5K electronics channels which can handle hit rates of up to 100 kHz per channel.

L. Present Status of the FT Project

The Toward Tagger system is being designed and built by a collaboration of several institutions including, the Italian National Institute for Nuclear Physics (INFN), the French Commissariat à l'Energie Atomique (CEA), the University of Edinburgh, the James Madison University, the Norfolk State University, the University of Ohio, and Jefferson Lab. Funds for the construction of the FT-Cal will be provided by INFN, while funds for the construction of the FT-Hodo and FT-Trk were requested via an MRI that was submitted to NSF in January 2012. Additional financial contributions will be provided by Jefferson Lab, the University of Edinburgh and by the European Commission via the FP7-HP3 project.

The conceptual design of the detector has been fully developed and R&D on the different components has been in progress for more than two years with the aim of finalizing the detector technical design and start the construction phase within 2012. To validate the proposed design of the FT-Cal and FT-Hodo, prototypes were built and installed in Hall B for a test with electron beam in December 2011. The FT-Cal prototype consisted of a 3×3 matrix of PbWO crystals, read-out with 10×10 mm^2 LAAPDs by Hamamatsu. The mechanical structure to support and thermally stabilize the crystals as well as the front-end electronics was based on the layout developed for the full FT-Cal. The hodoscope prototypes consisted of plastic scintillator tiles of various sizes and thickness, connected to different numbers of WLS fibers for the light collection. The fiber were coupled to the Hamamatsu 3×3 mm^2 SIPM that was selected for this detector system. The SIPM signal was amplified with a preamplifier prototype and readout with the same front-end electronics used for the calorimeter prototype. The FT-HODO prototype was installed in front of the FT-Cal prototype to intercept the trajectories of electrons hitting the central crystal of the calorimeter matrix. The test data are presently being analyzed but initial results showed that the observed signals from both prototypes are consistent with the expectations. Preliminary estimate of the FT-Cal prototype energy response indicated a resolution below 3% can be achieved for electron energy of $\sim$ 1.2 GeV. Further tests of improved FT-Cal and FT-Hodo prototypes are planned at the LNF Beam Test Facility [49] in May 2012. These new measurements will allow to determine energy and time resolution and test calibration procedures for both systems. R&D on the FT-Trk is in progress at CEA-Saclay in conjunction with the development of the Micromegas tracker for the CLAS12 Central Detector.

The layout and structure of these detectors are very similar and will allow to exploit the experience gained in the development of the central detector tracker to define the layout of the FT tracker. First test on micromegas prototypes were completed showing that the mechanical characteristics are within specifications and that the measured gain and response to cosmic rays are consistent with expectations.

M. Triggers

To positively identify the ground-state $\Xi^-(1320)$, at a minimum both K^+'s need to be detected. This gives us the state determination through missing mass. The same holds for higher mass Cascade states as well, though in practice a third detected particle can be used for background reduction. Consider the following reaction:

$$\begin{aligned} \gamma\, p \rightarrow \Xi^{*-}\, K^+\, K^+ \\ \hookrightarrow \Lambda\, K^- \\ \hookrightarrow p\, \pi^-. \end{aligned} \tag{12}$$

The Ξ^{*-} can be identified by the missing mass off K^+K^+ or by the invariant mass of the p K^- π^- final states. This is the general nature of $\Delta S = 2$ reactions. For the Ω^- state, any analysis will require at least three detected particles. The ground state reaction looks like:

$$\begin{aligned} \gamma\, p \rightarrow \Omega^-\, K^+\, K^+\, K^0 \\ \hookrightarrow \Lambda\, K^- \\ \hookrightarrow p\, \pi^-, \end{aligned} \tag{13}$$

where the K^0 typically goes to two pions. Here, the minimum final-state detection of the Ω^- can be done with the invariant mass of p K^- π^-. Therefore, this proposal's trigger is included the exotic-meson proposal's two-track trigger[20] and can run parasitically in this respect.

VI. BEAM TIME REQUEST AND EXPECTED RESULTS

Overall, it looks that it is feasible to measure the $\gamma p \rightarrow \Omega^- K^+ K^+ K^0$ cross section with CLAS12 without and with FT facility. While FT facility is critical for both cross section and polarization measurements for the $\gamma p \rightarrow \Xi^- K^+ K^+$.

VII. SUMMARY

...

[1] K. Nakamura *et al.* (Particle Data Group), J. Phys. G **37**, 075021 (2010).

[2] M. Gell-Mann and Y. Ne'eman, *The Eight-fold Way* (W.A. Benjamin, Inc. NY, 1964).

[3] V.E. Barnes *et al.*, Phys. Rev. Lett. **12**, 204 (1964).

[4] M. Deutschmann *et al.* (Aachen-Berlin-CERN-Innsbruck-London-Vienna Collaboration), Phys. Lett. **73B**, 96 (1978); M. Baublillier *et al.*, Phys. Lett. **78B**, 342 (1978).

[5] B. Aubert *et al.* (BaBar Collaboration), Phys. Rev. Lett. **97**, 112001 (2006).

[6] J.K. Hassall *et al.*, Nucl. Phys. *B189*, 397 (1981).

[7] D. Aston *et al.*, Phys. Rev. D **32**, 2270 (1985).

[8] K. Abe *et al.* (SLAC Hybrid Facility Photon Collaboration), Phys. Rev. D **32**, 2869 (1985).

[9] S. Capstick and N. Isgur, Phys. Rev. D **34**, 2809 (1986).

[10] L. Guo *et al.* (CLAS Collaboration), Phys. Rev. C **76**, 025208 (2007).

[11] K. Nakayama, Y. Oh, and H. Haberzettl, Phys. Rev. C **74**, 035205 (2006).

[12] B. Aubert *et al.* (BarBar Collaboration), Phys. Rev. D **78**, 034008 (2008).

[13] Adamovich *et al.* (W89 Collaboration), Eur. Phys. J. C **5**, 621 (1998).

[14] R.K. Bradford *et al.* (CLAS Collaboration), Phys. Rev. C **75**, 035205 (2007).

[15] M.E. McCracken *et al.* (CLAS Collaboration), Phys. Rev. C **81**, 025201 (2010).

[16] S. Brodsky, private communication, 2009.

[17] A. Radyushkin, private communication, 2009.

[18] J. Badier *et al.* (NA3 Collaboration), Phys. Lett. B **114**, 457 (1982).

[19] R. Vogt and S.J. Brodsky, Phys. Lett. B **349**, 569 (1995).

[20] *Meson spectroscopy with low Q^2 electronscattering in CLAS12*, Spokespersons: M. Battaglieri, R. De Vita, D.I. Glazier, C. Salgado, S. Stepanyan, and D. Weygand, JLab Proposal PR–11–005, Newport News, VA, USA, 2011.

[21] S.F. Biagi *et al.*, Z. Phys. C **34**, 175 (1987).

[22] V.G. Baryshevsky, K.G. Batrakov, and S. Cherkas, J. Phys. G **24**, 2049 (1998).

[23] N. Byers and S. Fenster, Phys. Rev. Lett. **11**, 52 (1963).

[24] K. Nakayama, Yongseok Oh, and H. Haberzettl, arXiv:1201.5598 [hep–ph]

[25] J.K. Ahn *et al.*, Phys. Lett. **B633**, 214 (2006).

[26] G.R. Charlton, Phys. Lett. B **32**, 720 (1970).

[27] R.D.A. Dalmeijer *et al.*, Nuovo Cimento Letters **4**, 373 (1970).

[28] R.A. Muller, Phys. Lett. **B38**, 123 (1972).

[29] J.M. Hauptman *et al.*, Nucl. Phys. **B125**, 29 (1977).

[30] Y. Fujiwara, C. Nakamoto, and Y. Suzuki, Prog. Theor. Phys. **94**, 353 (1995).

[31] Y. Fujiwara, C. Nakamoto, and Y. Suzuki, Phys. Rev. Lett. **76**, 2242 (1996).

[32] Y. Fujiwara, C. Nakamoto, and Y. Suzuki, Phys. Rev. C **54**, 2180 (1996).

[33] C. Nakamoto, Y. Fujiwara, and Y. Suzuki, Nucl. Phys. **A639**, 51c (1998).

[34] Y. Fujiwara, M. Kohno, C. Nakamoto, and Y. Suzuki, Phys. Rev. C **64**, 054001 (2001).

[35] S.B. Treiman, Phys. Rev. 113, 355 (1959).

[36] H.J. Lipkin and F. Scheck, Phys. Rev. Lett. **16**, 71 (1966).

[37] J. Schaffner-Bielich, Nucl. Phys. **A804**, 309 (2008).

[38] S.V. Bashinsky and R.L. Jaffe, Nucl. Phys. **A625**, 167 (1997).

[39] S.D. Paganis, T. Udagawa, G.W. Hoffmann, and R.L. Ray, Phys. Rev. C **56**, 570 (1997).

[40] W. Roberts and M. Pervin, Int. J. Mod. Phys. A **23**, 2817 (2008); M. Pervin and W. Roberts, Phys. Rev. C **77**, 025202 (2008).

[41] I. Akushevich, H. Bottcher, and D. Ryckbosch, arXiv:hep-ph/9906408.

[42] M. Dugger, http://www.jlab.org/Hall-B/secure/clas12/omegaMinus/ASU/vsGenBriefDescription.pdf

[43] ..., Spokespersons: xxx, JLab Proposal PR–xx–0xx, Newport News, VA, USA, 20xx.

[44] ..., Spokespersons: ..., JLab Proposal PR–xx–0xx, Newport News, VA, USA, 20xx.

[45] Nefkens95

[46] Duncan97

[47] Delbourgo99

[48] Fanti00

[49] G. Mazzitelli *et al.*, Nucl. Instrum. and Meth. A **515**, 524 (2003).